NASA TECHNICAL MEMORANDUM

NASA TM X-71672

NASA TM X-71672

SPINNING MODE SOUND PROPAGATION IN DUCTS WITH ACOUSTIC TREATMENT AND SHEARED FLOW

by Edward J. Rice
Lewis Research Center
Cleveland, Ohio 44135

TECHNICAL PAPER proposed for presentation at
Second Aeroacoustics Specialists Conference sponsored by
the American Institute of Aeronautics and Astronautics
Hampton, Virginia, March 24-26, 1975

SPINNING MODE SOUND PROPAGATION IN DUCTS WITH ACOUSTIC TREATMENT AND SHEARED FLOW

Edward J. Rice
Lewis Research Center
National Aeronautics and Space Administration
Cleveland, Ohio

E-8261

Summary

The propagation of spinning mode sound was considered for a cylindrical duct with sheared steady flow. The calculations concentrated on the determination of the wall optimum acoustic impedance and the maximum possible attenuation. Both the least attenuated and higher radial modes for spinning lobe patterns were considered. A parametric study was conducted over a wide range of Mach numbers, spinning lobe numbers, sound frequency, and boundary layer thickness. A correlation equation was developed from theoretical considerations starting with the thin boundary layer approximation of Eversman. This correlation agrees well with the more exact calculations for inlets and provides a single boundary layer refraction parameter which determines the change in optimum wall impedance due to refraction effects.

Introduction

Noise attenuation data using inlet suppressors, with wall treatment only, have pointed out two phenomena which have required additional study. First, the noise attenuation was much larger than had been anticipated from flow duct tests or from axisymmetric sound propagation theory. Second, large attenuations were observed with much higher porosity (low acoustic resistance) acoustic liners than would have been anticipated from previous optimization studies. A recent parametric study of the optimum wall impedance for the least attenuated spinning mode[1] has shown that spinning modes could be anticipated to attenuate much faster than axisymmetric modes in an inlet with wall treatment only. This has helped explain the first point raised above. It was suspected that the bulk of the answer to the second point above involved the effect of the steady flow inlet boundary layer on the optimum wall impedance. This study was thus initiated to extend the work of Ref. 1 (spinning mode propagation with acoustic treatment) to include the boundary layer effects. This paper will concentrate on the optimum wall impedance and maximum possible sound attenuation and the correlation of these results with the pertinent variables involved.

The effect of boundary layers on sound propagation in acoustically lined ducts has been considered in the past for axisymmetric mode (nonspinning) propagation (e.g., Refs. 2 and 3), and an extensive bibliography and discussion of the recent papers on this subject is given in Ref. 4. Spinning mode sound propagation with an axially uniform boundary layer was presented in Ref. 5. Comparisons of theory and experimental data were presented showing reasonable agreement. The above studies are very important since they demonstrate the necessity of considering boundary layer effects, but they do not include a parametric study of the problem which can be immediately used for suppressor design purposes. Current interest in sound propagation with sheared flow is apparent in two recent papers.[6-7] Reference 6 presents a parametric study of the optimum impedance using the least attenuated axisymmetric mode. Some calculations are presented for spinning modes. Reference 7 presents spinning mode calculations but no optimization is attempted.

The purpose of this paper is to present a parametric study and a correlation of the results for the effect of axially uniform boundary layers on the propagation of spinning mode sound in an acoustically lined cylindrical duct. A wide variation of steady flow Mach number, boundary layer thickness, sound frequency parameter, and spinning lobe number were considered. The emphasis was on the least attenuated radial mode for the various spinning lobe numbers; however, the second and fifth radial modes for a seven lobe pattern were also analyzed.

The analysis consisted of locating the optimum wall impedance (at which maximum possible sound attenuation occurs) for the previously discussed wide range of variables.

A major objective of this study was to obtain a correlating equation to unify the results of the parametric study. Since the correlation is quite complicated, approximate expressions are developed that more clearly demonstrate the effect of the variables involved and that are sufficiently accurate for first estimates in acoustic liner design.

Symbols

$\bar{A}$ specific acoustic admittance ($1/\zeta$)

$\bar{A}_0$ specific acoustic admittance - uniform or slip flow

B_θ optimum resistance coefficient for circular duct with slip flow (see Eq. (32) and Table I)

B_χ optimum reactance coefficient for circular duct with slip flow (see Eq. (33) and Table I)

c speed of sound, m/sec

D circular duct diameter, m

F boundary layer refraction function (see Eq. (27))

f frequency, Hz

G boundary layer shape function ($G = (y/\delta)^{1/7}$ for $1/7^{th}$ power profile)

I_1 integral function across boundary layer (see Eq. (A-6))

I_2 integral function across boundary layer (see Eq. (A-7) or Eq. (28) for $1/7^{th}$ power profile)

i $\sqrt{-1}$

J_m Bessel function of first kind of order m

K factor in axial wave number, see Eqs. (3), (9), and (10)

k ω/c, m^{-1}

M axial steady flow Mach number (function of radial coordinate)

M_0 axial steady flow Mach number - free stream uniform value

m spinning mode lobe number

P acoustic pressure, N/m^2

p part of acoustic pressure which is function of radial coordinate (see Eq. (3)), N/m^2

Q $1 + iM_0(\sigma + i\tau)$ or $1 - MK_0$

R amplitude of eigenvalue α

$\mathcal{R}$ ratio of optimum resistance to optimum reactance for uniform flow (no boundary layer), $-\theta_0/\chi_0$

r radial coordinate, m

r_0 circular duct radius, m

t time, sec

V axial steady flow velocity (function of radial coordinate), m/sec

V_0 axial steady flow velocity - free stream value, m/sec

v acoustic particle velocity (vector), m/sec

x axial coordinate, m

y distance from the wall in the boundary layer, m

$\bar{y}$ nondimensional distance from the wall in the boundary layer (y/δ)

Z acoustic impedance (P/v_r), $kg/m^2/sec$

α complex radial eigenvalue ($\alpha = R^{i\varphi}$)

$\bar{\alpha}$ dimensionless quantity (see Eq. (A-4), appendix)

β $\alpha(1 - \delta/r_0)$

$\bar{\beta}$ dimensionless quantity (see Eq. (A-3))

δ boundary layer thickness, m

δ^* boundary layer displacement thickness, m

ϵ dimensionless boundary layer thickness, δ/r_0

ζ specific acoustic impedance (also used for optimum value with a finite boundary layer thickness)

ζ_0 optimum specific acoustic impedance with zero boundary layer thickness (slip flow at wall)

η frequency parameter (fD/c)

θ specific acoustic resistance, Real (ζ)

θ_0 optimum specific acoustic resistance when $\delta = 0$, Real (ζ_0)

$\bar{\theta}$ boundary layer momentum thickness, m

λ sound wavelength, m

ν kinematic viscosity, m^2/sec

ξ nondimensional radial coordinate (r/r_0)

ρ density, kg/m^3

σ attenuation coefficient (see Eq. (10))

σ_0 maximum possible attenuation coefficient when $\delta = 0$

τ propagation coefficient (see Eq. (10))

Φ angular coordinate, rad

φ phase of eigenvalue, α, deg

χ specific acoustic reactance, Imag (ζ)

χ_0 optimum specific acoustic reactance when $\delta = 0$, Imag (ζ_0)

ω circular frequency, rad/sec

Subscripts:

j indicate j^{th} radial mode

r radial component

Theoretical Model

In the following sections the analytical approach will be outlined. The standard sound propagation theory will first be reviewed to establish the methods and terminology used in this paper. The method of obtaining the least attenuated mode optimum impedance will then be presented. Calculated results of the parametric study with boundary layers will next be presented followed by the correlation equations which unify all of the calculated results. Finally, some approximate expressions will be developed which are useful in illuminating the roles of the several variables considered here.

The geometry and steady flow profile considered here are as shown in Fig. 1. The duct is circular with no splitter rings or hub. The boundary layer velocity

profile is linear near the wall and has a $1/7^{th}$ power dependence outside of this linear region. The steady flow is assumed to be uniform in the central region of the duct outside of the boundary layer.

Spinning Mode Propagation Theory With a Boundary Layer

Certain assumptions are common in all of the theoretical development which follows. Only in the boundary layer are steady flow gradients considered. The soft walls are assumed point reacting and of uniform impedance. These assumptions imply that no waves propagate within the liner backing cavity (prevented by honeycomb cells), and that any perforations are closely spaced compared to a wavelength of sound. No end reflections are considered; that is, the soft duct is sufficiently long to render the reflections at the duct termination unimportant or the mode is well enough cut on so that no end reflection will occur. A cut-on mode is defined here as a propagating mode; the frequency parameter (η) is sufficiently high so that axial propagation occurs. Only very near cut-off will this assumption (no end reflection) be a problem. Below cut-off the modes carry very little energy due to their out-of-phase pressure-velocity relationship, and well above cut-off the end impedance[9] is such that very little reflection will occur. It is further assumed that the sound pressure level is sufficiently low so that the linearized acoustic wave equation is valid. The linearized equations should be adequate except perhaps very near the rotor, when shock waves are generated, or where near sonic flows exist.

The wave equation with transverse (perpendicular to wall) steady flow gradients is given by:[3]

$$\frac{1}{c^2}\frac{\partial^2 P}{\partial t^2} + \frac{2M}{c}\frac{\partial^2 P}{\partial x\,\partial t} + M^2\frac{\partial^2 P}{\partial x^2} - 2\rho c\frac{\partial M}{\partial r}\frac{\partial v_r}{\partial x} - \nabla^2 P = 0 \tag{1}$$

where in cylindrical coordinates

$$\nabla^2 P = \frac{\partial^2 P}{\partial r^2} + \frac{1}{r}\frac{\partial P}{\partial r} + \frac{1}{r^2}\frac{\partial^2 P}{\partial \Phi^2} + \frac{\partial^2 P}{\partial x^2} = 0 \tag{2}$$

Solutions are sought in the form:

$$P = p(r)e^{i\omega t - im\Phi - ikKx} \tag{3}$$

Combining Eqs. (1) to (3) yields

$$\frac{d^2 P}{dr^2} + \frac{1}{r}\left[1 + \frac{2Kr}{(1 - MK)}\frac{dM}{dr}\right]\frac{dp}{dr} + \left\{k^2\left[(1 - MK)^2 - K^2\right] - \frac{m^2}{r^2}\right\}P = 0 \tag{4}$$

where $k = \omega/c$, and use was made of the momentum equation

$$v_r = \frac{i}{\rho\omega(1 - MK)}\frac{\partial p}{\partial r} \tag{5}$$

Defining a nondimensional radial variable

$$\xi = \frac{r}{r_0} \tag{6}$$

where r_0 = outer wall radius, Eq. (4) becomes

$$\frac{d^2 p}{d\xi^2} + \frac{1}{\xi}\left[1 + \frac{2K\xi}{(1 - MK)}\frac{dM}{d\xi}\right]\frac{dp}{d\xi} + \left\{(\pi\eta)^2\left[(1 - MK)^2 - K^2\right] - \frac{m^2}{\xi^2}\right\}p = 0 \tag{7}$$

where the frequency parameter

$$\eta = \frac{\omega r_0}{\pi c} = \frac{fD}{c} \tag{8}$$

Defining K as

$$K = \tau - i\sigma \tag{9}$$

gives for the axial exponent,

$$-ikKx = -k(\sigma + i\tau)x \tag{10}$$

which indicates that the attenuation is determined by σ, and the axial propagation speed is inversely proportional to τ.

Uniform velocity region. In the central uniform velocity region [$\xi \le 1 - (\delta/r_0)$ or $r \le r_0 - \delta$], the Mach number gradient disappears ($dM/d\xi = 0$) and Eq. (7) becomes Bessels' differential equation with standard modal solutions

$$p_j = J_m(\alpha_j \xi) \tag{11}$$

where the j subscript indicates that an infinite set of modal solutions are possible. This discussion will be restricted to the least attenuated radial mode and the j will be dropped for brevity. The attenuation and propagation coefficients are related to the eigenvalue α by

$$\sigma + i\tau = \frac{-iM_0 + i\sqrt{1 - \left(1 - M_0^2\right)\left(\frac{\alpha}{\pi\eta}\right)^2}}{1 - M_0^2} \tag{12}$$

The ratio of the pressure slope to the pressure evaluated at the boundary layer, is given by

$$\left.\frac{dp/d\xi}{p}\right]_{\xi = 1 - (\delta/r_0)} = \frac{m - \beta\frac{J_{m+1}(\beta)}{J_m(\beta)}}{1 - \frac{\delta}{r_0}} \tag{13}$$

which provides the boundary condition to start the Runge-Kutta integration in the boundary layer and where

$$\beta = \alpha\left(1 - \frac{\delta}{r_0}\right) \tag{14}$$

When the boundary layer is ignored (slip condition at the wall), continuity of particle displacement is used at the wall. The specific acoustic impedance result is

$$\zeta = \frac{i\pi\eta Q^2}{\alpha \dfrac{J_{m+1}(\alpha)}{J_m(\alpha)} - m} \tag{15}$$

where

$$Q = 1 + iM_0(\sigma + i\tau) = 1 - M_0 K \tag{16}$$

Boundary layer region. When a velocity gradient exists, closed form solutions of Eq. (7) do not exist except for special cases such as a linear velocity profile.[10] Thus a Runge-Kutta integration of Eq. (7) was performed over the boundary layer with Eq. (13) as a starting point. More detail will be given in the Calculation Procedure section. The boundary layer profile was assumed to be linear near the wall with a $1/7^{th}$ power relation used over the rest of the boundary layer.

At the wall $M = 0$, and the specific acoustic wall impedance can be calculated from

$$\zeta = \left.\frac{-i\pi\eta p}{dp/d\xi}\right]_{\xi=1} \tag{17}$$

where p and $dp/d\xi$ at $\xi = 1$ are provided by the Runge-Kutta integration process.

Boundary Layer Velocity Profile

It was concluded in Ref. 11 that a linear velocity profile with slip could be used to approximate the actual turbulent velocity profile. This would provide an adequate approximation if the boundary layer shape factor (δ^*/θ) and displacement thickness (δ^*) were matched. This procedure greatly reduces the number of points required in the integration and is probably the sensible procedure to follow when a great number of calculations are to be made. In this paper, however, a limited number of calculations were intended with the results being correlated for future use. The more conventional approach using an adequate description of the entire boundary layer was thus used to eliminate the possibility of an unforeseen error due to an unnecessary assumption. This did, however, require that at least 100 points be used in the Runge-Kutta integration across the boundary layer.

The following description of the boundary layer profile provides a wall shear stress that is commensurate with the free stream velocity and boundary layer thickness assumptions. The velocity profile near the wall was derived from shear stress considerations given in Ref. 12.

In the laminar sublayer near the wall the velocity profile can be expressed as

$$\frac{V}{V_0} = 0.0225\left(\frac{V_0\delta}{\nu}\right)^{3/4}\left(\frac{y}{\delta}\right) \tag{18}$$

where

$$y = r_0 - r \tag{19}$$

is the distance from the wall, V_0 is the free stream velocity, δ is the entire boundary layer thickness, and ν is the kinematic viscosity.

Outside of the laminar region the velocity profile was assumed to be

$$\frac{V}{V_0} = \left(\frac{y}{\delta}\right)^{1/7} \tag{20}$$

At

$$\frac{y}{\delta} = 83.8\left(\frac{V_0\delta}{\nu}\right)^{-7/8} \tag{21}$$

the velocity predicted by Eqs. (18) and (20) are equal and the transition from laminar to turbulent profile is made. A slight change in slope occurs at the transition point since no attempt was made to model the transition region.

The steady flow velocity and slope in the form necessary for use in Eq. (7) are in the laminar sublayer,

$$M = \frac{0.0225\, M_0 r_0}{\delta}\left(\frac{M_0 c\delta}{\nu}\right)^{3/4}(1 - \xi) \tag{22}$$

and

$$\frac{dM}{d\xi} = -\frac{0.0225\, M_0 r_0}{\delta}\left(\frac{M_0 c\delta}{\nu}\right)^{3/4} \tag{23}$$

and in the turbulent region,

$$M = M_0\left[\frac{r_0}{\delta}(1 - \xi)\right]^{1/7} \tag{24}$$

and

$$\frac{dM}{d\xi} = -\frac{M}{7(1 - \xi)} \tag{25}$$

Note that in the laminar sublayer the boundary layer thickness (δ) occurs in the Reynolds number $(M_0 c\delta/\nu)$

without duct size (r_0) scaling. Thus the laminar profile does not precisely scale with duct size and the size of the duct must be specified. For all calculations in this paper a duct radius of $r_0 = 0.815$ meter (36 in.) was used. The scaling error should be small since the laminar region is only 2 percent or less of the boundary layer for typical Reynolds numbers of interest.

It should be recognized that any velocity profile used is an approximation since the effect of an acoustic liner on the profile near the wall is not known at this time.

Calculation Procedure

The calculation procedure will be outlined first for the uniform flow case (no boundary layer) since the philosophy can be most easily explained and the boundary layer case is then a simple extension.

Uniform Flow

The intention here is to generate constant attenuation curves in the wall impedance plane for a particular mode. Where the closed curves of constant damping degenerate to a point, the maximum possible sound power attenuation is determined as well as the optimum wall impedance. This procedure for the uniform flow case without boundary layers is explained here and illustrated in Fig. 2 for $M_0 = -0.4$, $\eta = 10$, and $m = 7$.

First a desired constant damping value is selected (such as $\sigma = 0.01$ in Fig. 2). Next, a series of propagation coefficients τ values are selected. These are in turn (along with σ) used in Eq. (12) to calculate the eigenvalue α, then Q (Eq. (16)), and finally the acoustic impedance ζ from Eq. (15). Each impedance value ($\theta + i\chi = \zeta$) is normalized by η and plotted in Fig. 2. By selecting a new damping value (σ) the series of contours are generated. The optimum impedance and maximum damping occur where the tear-drop shaped contours degenerate to a point.

Boundary Layer

A similar procedure to that of the uniform flow case is followed with a boundary layer. Again σ and τ are selected and Eq. (12) is used to calculate the eigenvalue α. Equations (13) and (14) are used to calculate $1/p\ dp/d\xi$ at the boundary layer edge. This pressure-pressure slope value is used to start the Runge-Kutta integration through the boundary layer. This integration transforms $1/p\ dp/d\xi$ at the boundary layer edge to $1/p\ dp/d\xi$ at the wall. Equation (17) is then used to calculate the wall impedance. This amounts to using the standard well known solution (Eq. (11)) in the uniform flow region and deriving from this solution the boundary conditions necessary for the unknown solution for propagation in the boundary layer described by Eq. (7). This procedure is very efficient since numerical integration is necessary over only a small portion of the duct (the boundary layer). Also modal correspondence or identification is quite simple since a predetermined mode is specified in the uniform flow region. This procedure is similar to that used in Ref. 5.

Equation (7) is solved by Runge-Kutta integration (using 100 steps) through the boundary layer using Eqs. (22) to (25) to specify the Mach number and its slope. When the wall is reached in the integration, the pressure and its slope are used in Eq. (17) to calculate the required wall impedance.

Sample results of this calculation are shown in Fig. 3. These are similar to the curves of Fig. 2 except that only a single damping value curve is shown for each boundary layer thickness. The optimum impedance is found within each one of these contours and can be estimated by the impedance value at the round tip of the tear-drop shaped contour. For the results presented in the next section the contours were further refined from those shown in Fig. 3. However, even for the sample curves shown here, it is evident that an extremely large drop in optimum resistance occurs when the boundary layer is increased.

Results of Calculations

The calculation procedure described in the previous section was exercised with a wide range of input variables. Mach numbers from -0.8 (inlet) to +0.6 (exhaust), spinning lobe numbers (m) from 3 to 50, frequency parameters (η) from 5 to 50, and boundary layers up to 30 percent of the radius were used. The purpose of this section is just to present the results and point out the extreme magnitude of the boundary layer effect in the inlet (negative Mach number). The effect in the exhaust duct is much more moderate. Since the results are from a numerical integration where no closed form solution exists, they may be looked upon as extremely repeatable computer experiments of limited use, except to note trends, until they are unified and correlated. The correlation of the results will be performed in the next section.

The results of interest in this paper are the optimum acoustic impedance and the maximum possible sound power attenuation obtained at this optimum impedance. This section contains results only for the least attenuated spinning modes. Higher order radial modes are deferred to a later section. Note also that the frequency parameter (η) is always selected so that the modes propagate. This was done to simplify the correlation procedure and not because of limitations of the calculation

procedure. Also propagating modes are usually of most interest.

The following results have been normalized by their counterpart with no boundary layer. This will increase the ease of use since the zero boundary layer thickness results are quite easily obtained.

Inlet Conditions - Negative Mach Number

Figure 4 shows the results for the optimum resistance ratio as a function of boundary layer - wavelength ratio for negative Mach numbers (inlets). This ratio compares the optimum resistance with and without a boundary layer. Note that the full boundary layer thickness is used here. If displacement thickness (δ^*) were desired instead it could be estimated as $\delta/8$. Note the extreme reduction of optimum resistance with increasing boundary layer thickness particularly for large Mach numbers and frequency parameters. Note also that there is a frequency effect beyond that of wavelength which is accounted for in the abscissa (δ/λ). Also the Mach number effect cannot be simply accounted for by using an effective wavelength $[\lambda(1 + M_0)]$.

Spinning lobe number (m) has an effect upon θ/θ_0 but this effect is not so dramatic as that of inlet Mach number or frequency. It will be found in the next section that these curves are all similar in shape with the roll-off value of δ/λ being a function of the variables involved.

A sample of the optimum reactance ratio is shown in Fig. 5 as a function of δ/λ for $m = 7$, $\eta = 10$, and for several inlet Mach numbers. The results (for a given M_0) increase at first to about double the $\delta/\lambda = 0$ value ($\chi/\chi_0 = 1$) and then gradually fall off with increasing boundary layer thickness. Note that both χ and χ_0 are negative.

The change in mode damping (α) is shown in Fig. 6. The maximum possible attenuation falls off very little until extremely large boundary layers are encountered. This implies that if the optimum impedance could be properly accounted for in a liner design, the peak attenuation need not suffer much of a loss due to the boundary layer.

Exhaust Conditions - Positive Mach Number

Figures 7(a), (b), and (c) contain calculated results for optimum resistance, reactance, and damping for positive Mach number. These results were calculated with seven spinning lobes ($m = 7$), $\eta = 10$, and $M_0 = +0.6$. The boundary layers contained in the span of the abscissa were from 1/2 to 20 percent of the duct radius.

In spite of the large Mach number and range of boundary layer thickness, not much change occurs in the optimum resistance ratio ($0.96 \leq \theta/\theta_0 \leq 1.05$). Recall that for the same conditions ($m = 7$, $\eta = 10$) for an inlet ($M_0 = -0.6$) the optimum resistance ratio changes by several orders of magnitude as δ/λ was varied over a similar range (see Fig. 4). Although the reactance appears to change substantially, this is due to the method of presentation as a ratio. The actual reactance changes from about -0.31 to zero in this boundary layer thickness range. The maximum damping ratio starts to increase somewhat at $\delta/\lambda = 0.25$ ($\delta/r_0 = 0.05$) and has increased by only 30 percent at $\delta/\lambda = 1$ ($\delta/r_0 = 0.2$) which represents an extremely large boundary layer.

It should be recognized that the model used here is not necessarily valid for an exhaust duct. Exhaust ducts are usually annular and the velocity profile is probably dominated by the rotor and stator properties rather than a simple boundary layer. The conclusion to be drawn here should be that all things being equal (except the flow direction) the exhaust duct optimum impedance is much less sensitive to sound refraction effects than is the inlet optimum impedance.

Correlation of Results

The correlating equations discussed below are derived in the appendix where assumptions leading to the correlations, deletions, and empirical corrections are discussed. The correlations are considered for inlets (negative Mach number) only since there the boundary layer effects are large while they are small for exhaust ducts. First, the complete correlation equations are presented which provide a very adequate unification of the calculations described in a previous section. Since these expressions are still quite complicated it is valuable to look at more approximate expressions which better show the effects of the variables involved.

Complete Correlations

The expression for the optimum acoustic impedance for spinning modes in a circular inlet ($M_0 \leq 0$) with steady sheared flow is given by (see appendix)

$$\zeta = \frac{(1 + \epsilon)\zeta_0}{1 - iF\zeta_0} \tag{26}$$

where ζ_0 is the optimum acoustic impedance without a boundary layer (slip flow), $\epsilon = \delta/r_0$, and F is the expression

$$F = \frac{\pi(\delta/\lambda)}{4I_2(1 + M_0)^2}\left[M_0(1 - 2M_0) - 4(1 + 2M_0)(1 + M_0)\left(\frac{m}{\pi\eta}\right)^2\right] \tag{27}$$

The quantity I_2 contains all of the boundary layer shape

information and for a $1/7^{th}$ power velocity profile is expressed as

$$L_2 = \frac{1 + \frac{M_0}{4}\left(1 + \frac{M_0}{9}\right)}{(1 + M_0)^2} \tag{28}$$

The quantity in the denominator of Eq. (27) is then

$$L_2(1 + M_0)^2 = 1 + \frac{M_0}{4}\left(1 + \frac{M_0}{9}\right) \approx 1 + \frac{M_0}{4} \tag{29}$$

The last term in the brackets in Eq. (27) is generally small (identically zero at $M_0 = -0.5$) and most of the lobe number (m) effect is carried in the ζ_0 term in Eq. (26).

Equation (26) can be further reduced by taking real and imaginary parts yielding

$$\frac{\theta}{\theta_0} = \frac{1 + \epsilon}{1 + 2F\chi_0 + F^2\left(\theta_0^2 + \chi_0^2\right)} \tag{30}$$

$$\frac{\chi}{\chi_0} = \frac{(1 + \epsilon)\left[1 + F\left(\frac{\theta_0^2}{\chi_0} + \chi_0\right)\right]}{1 + 2F\chi_0 + F^2\left(\theta_0^2 + \chi_0^2\right)} \tag{31}$$

The zero boundary layer thickness input parameters to Eqs. (26), (30), and (31) can be estimated from Ref. 1 as

$$\theta_0 \approx \frac{B_\theta \eta}{(1 + M_0)^2} \tag{32}$$

$$\chi_0 \approx \frac{-B_\chi \eta}{(1 + M_0)^2} \tag{33}$$

valid for propagating modes. The quantities B_θ and B_χ are found in Table I (reproduced from Ref. 1 for convenience) for the least attenuated spinning mode with m lobes.

Equations (30) and (31) were used along with Eqs. (27) and (28) to calculate the normalized resistance and reactance ratios using all of the conditions shown on Figs. 4 and 5. The results are shown in Figs. 8 and 9 as curves along with the previous more exact calculations shown as point symbols. The agreement is seen to be very adequate for the resistance ratio and quite acceptable for the reactance ratio. As discussed in the appendix, a slight empirical correction was made to the correlation equations to better fit the resistance ratio. No special measures were taken to fit the reactance.

A correlation was obtained for the damping of the least attenuated spinning mode calculations, samples of which were previously shown in Fig. 6. This correlation is completely empirical in contrast to those for the resistance and reactance ratios. The damping correlation is shown in Fig. 10 by the solid curve while the previously calculated points are shown as symbols. Again the results are shown as a ratio; maximum damping with a boundary layer divided by maximum damping with $\delta = 0$ (slip flow).

The correlation is given by

$$\frac{\sigma}{\sigma_0} = \frac{1}{1 + \frac{5M_0^2(\delta/\lambda)^2}{1 + M_0}} \tag{34}$$

The maximum attenuation ratio can also be calculated using Eq. (34), since the maximum attenuation is proportional to the damping coefficient for single modes.[1] Zero boundary layer thickness maximum attenuations for spinning modes are found in Ref. 1.

Approximate Correlations

It is desirable to simplify the resistance and reactance correlations and reduce them to more universal or general curves. Single correlating curves can be obtained for the optimum resistance and reactance ratios with only a small loss in accuracy. This will be done in two steps. First some approximations will be made to collapse the optimum resistance and reactance ratio correlations, and second some more gross approximations will better reveal the effects of the major variables.

Acoustic Liner Design Correlations

In Table I it is apparent that $B_\theta \approx 4B_\chi$ which is fairly accurate except at m = 0 and 1 (the exact ratio of B_θ/B_χ could be used here). This implies that (see Eqs. (32) and (33))

$$\theta_0 \approx -4\chi_0 \tag{35}$$

This can be used in Eqs. (30) and (31) to derive

$$\frac{\theta}{\theta_0} \approx \frac{1}{1 - \frac{1}{2}F\theta_0 + (F\theta_0)^2} \tag{36}$$

and

$$\frac{\chi}{\chi_0} \approx \frac{1 - 4F\theta_0}{1 - \frac{1}{2}F\theta_0 + (F\theta_0)^2} \tag{37}$$

Now it is apparent that the optimum resistance and reactance ratios are functions of only a single quantity, $F\theta_0$. This quantity is used as the independent variable

to plot Eqs. (36) and (37) in Figs. 11 and 12 which also contain the previously developed calculated points. The collapse of the resistance calculations onto a single curve is seen to be very good in Fig. 11, while some scatter is seen in the reactance ratio for very large boundary layers in Fig. 12. Again, this reactance error is not significant for liner design purposes.

Note that F is negative for negative Mach number and thus $-F\theta_0$ was used in these two figures. The term $(-4F\theta_0)$ causes the initial increase in the reactance ratio while the term $(F\theta_0)^2$ causes the ultimate roll-off in both ratios.

Equations (36) and (37) should be sufficiently accurate for inlet liner design purposes. The quantity F is calculated from Eq. (27) and θ_0 is calculated from Eq. (32) using B_θ values from Table I.

Further Approximations to Illustrate the Effect of the Variables

It is interesting to look at the correlating equations for large $(-F\theta_0)$. Equations (36) and (37) can be written in the limiting forms

$$\left.\begin{aligned} \frac{\theta}{\theta_0} &\approx \frac{1}{(F\theta_0)^2} \\ \frac{\chi}{\chi_0} &\approx \frac{-4}{F\theta_0} \end{aligned}\right\} -F\theta_0 > 1 \qquad (38), (39)$$

Thus θ/θ_0 varies with the inverse square power and χ/χ_0 with the inverse of $(-F\theta_0)$. A comparison of Eqs. (38) and (39) with Figs. 11 and 12 show an adequate approximation for large $(-F\theta_0)$.

A rough approximation for B_θ as seen in Table I can be given by

$$B_\theta \approx \frac{0.8}{m^{1/2}} \qquad (m \neq 0) \qquad (40)$$

where m is the lobe number. This gives the approximation (using Eq. (32))

$$\theta_0 \approx \frac{0.8\,\eta}{m^{1/2}(1 + M_0)^2} \qquad (41)$$

Further assume that the first term in Eq. (27) dominates the second term. This assumption is usually true. Also drop the empirically determined term $1/2(1 - 2M_0)$, which is similar to one for most practical inlets. Then Eq. (27) yields

$$F \approx \frac{\pi M_0(\delta/\lambda)}{2L_2(1 + M_0)^2} \qquad (42)$$

Next use Eq. (29) and ignore the $M_0/4$ term. Therefore

$$F \approx \frac{\pi M_0}{2}\left(\frac{\delta}{\lambda}\right) \qquad (43)$$

Use Eq. (41) to obtain

$$F\theta_0 \approx \frac{0.4\,\pi M_0 \eta}{m^{1/2}(1 + M_0)^2}\left(\frac{\delta}{\lambda}\right) \qquad (44)$$

And finally from Eqs. (38) and (39)

$$\frac{\theta}{\theta_0} \approx 0.6\,m\left[\frac{(1 + M_0)^2}{M_0\eta(\delta/\lambda)}\right]^2 \qquad (45)$$

and

$$\frac{\chi}{\chi_0} \approx -\frac{3.2\sqrt{m}\,(1 + M_0)^2}{M_0\eta(\delta/\lambda)} \qquad (46)$$

Recall that these expressions are valid only for $(-F\theta_0) > 1$, and for the least attenuated spinning mode. Some observations can be made concerning the effect of boundary layer refraction on the optimum impedance of acoustic liners. Note that reductions in these equations mean increased refraction effects. The extreme sensitivity to inlet Mach number and to the frequency parameter to a slightly smaller extent are evident in the equations. This sensitivity was of course seen in the more exact calculated results. The higher the spinning lobe number the less the effect of sound refraction.

It is also interesting that there is a frequency effect beyond that found in δ/λ. Also it is not sufficient to use an effective wavelength $\lambda_{eff} = (1 + M_0)\lambda$ to account for the Mach number effect.

To determine whether these approximate expressions (Eqs. (45) and (46)) can be used and in fact whether boundary layer refraction must be considered, the nomograph of Fig. 13 can be used. This nomograph determines the values for which $(-F\theta_0) = 1$. For example, let $M_0 = -0.5$ and suppose a lobe pattern with 10 lobes is suspected. A value of $\eta^2\delta/\nu_0 = 2.25$ is read off the ordinate. Now suppose that the boundary layer displacement thickness is $0.0028\ r_0$. The boundary layer thickness for purposes of the present correlation is $\delta/r_0 = 0.0224$ ($\delta = 8\delta^*$ for $1/7^{th}$ power velocity profile). Thus $\eta^2 = 100$ or $\eta = 10$. For a frequency parameter above 10, the boundary layer refraction will cause sufficient change to alter the liner design and the regime of validity of Eqs. (45) and (46) is being approached.

Refraction Effect on Higher Order Radial Modes

The correlations presented in the previous section were for the least attenuated radial component of a spinning mode. It is of interest to determine whether the

correlation is sufficiently generalized to include propagating higher radial modes.

Equations (36) and (37) must be generalized to apply to the higher order radial modes. First Eq. (35) is altered to become

$$\theta_0 \approx -\mathcal{R}\chi_0 \tag{47}$$

where $\mathcal{R}$ was 4 for the least attenuated radial mode but is higher than 4 for the higher radial modes. The analogies to Eqs. (36) and (37) can then be easily derived from Eqs. (30) and (31) and are expressed as

$$\frac{\theta}{\theta_0} \approx \frac{1}{1 - \frac{2}{\mathcal{R}} F\theta_0 + (F\theta_0)^2} \tag{48}$$

and

$$\frac{\chi}{\chi_0} \approx \frac{1 - RF\theta_0}{1 - \frac{2}{\mathcal{R}} F\theta_0 + (F\theta_0)^2} \tag{49}$$

These expressions are shown as curves on Figs. 14 and 15 along with the exact calculations for the second and fifth radial modes of a seven-lobe spinning mode. For the second radial mode $\mathcal{R} = 5.9$ and for the fifth radial mode $\mathcal{R} = 10.1$ was used. The agreement between the exact calculations and the correlations are seen to be excellent for the optimum resistance ratio over the entire $(-F\theta_0)$ range, while the optimum reactance ratio deviates somewhat for higher values of $(-F\theta_0)$, as did the optimum reactance ratio for the least attenuated mode. The reactance correlation could easily be improved if it were considered necessary. A slight error in reactance is not critical in a liner design since it will only slightly change the frequency at which peak attenuation occurs. Resistance is much more critical since it will determine if the maximum attenuation can be approached at all, and the effect of a boundary layer on the optimum resistance is much greater than on the optimum reactance.

Because of the way in which the correlating equations are normalized they seem to have general validity for any propagating mode. This normalization involves the use of the zero boundary layer or slip-flow solutions.

Discussion of Boundary Layer Refraction Parameter

It is apparent from the previous discussions of results that the single parameter $(-F\theta_0)$ pretty well determines the boundary layer refraction effects which become important when $-F\theta_0 > 1$ for an inlet. The discussion will be limited here to the alteration of the optimum resistance which is by far the dominant effect.

It is interesting to look at the parameter in the following form

$$-F\theta_0 \approx \left[\frac{-\pi M_0(\delta/\lambda)}{2I_2(1 + M_0)^2}\right]\left[\frac{B_\theta \eta}{(1 + M_0)^2}\right] \tag{50}$$

Increases in the bracketed quantities in Eq. (50) will increase the boundary layer refraction effect and the inverse is also true. The parameters which obviously increase refraction effects are increased boundary layer thickness (δ), increased frequency (through both λ and η), and increasingly negative Mach number (inlets). At high negative Mach number, the $(1 + M_0)^2$ quantity is by far the dominant term. Recall that I_2 roughly cancels one of the $(1 + M_0)^2$ terms (see Eq. (29)). More subtle effects occur due to the B_θ term. The quantity B_θ is seen to decrease with increasing lobe number (m) in table I, and for any given value of (m), B_θ also decreases with higher order radial mode number. Thus the effect of boundary layer refraction is diminished for higher order spinning and radial mode numbers.

All of the boundary layer shape information is contained in the integral I_2 (see appendix). Since all of the results in this paper were for similar velocity profiles, no quantitative statements about I_2 will be made at this time.

Although no claims have been made about the optimum resistance and reactance ratio correlations fitting the exhaust duct optimization calculations, the development in the appendix was general until the small empiricism was added. Equation (50) does not contain the empiricism and could be easily altered for use with positive Mach number by dropping the minus signs. Recall that only qualitative approximations are considered here. The quantities δ, λ, η, and B_θ have the same effect as in the inlet case, and I_2 still roughly cancels one of the $(1 + M_0)^2$ terms. However, the remaining $(1 + M_0)^2$ term now decreases $F\theta_0$ instead of increasing it as in the inlet case. For instance, the ratio of the $F\theta_0$ values between minus and plus Mach numbers at $|M_0| = 0.5$ is a factor of 9. Thus the boundary layer in the exhaust duct would have to be nine times that in the inlet duct (all other terms being equal) to start producing a significant refraction effect. The divergence between the two cases $(\pm M_0)$ is even more pronounced than the simple calculation above suggests. This can be seen in Eq. (36). For inlets, the $-(1/2)F\theta_0$ term is actually positive and both terms in the denominator cause a fall-off in θ/θ_0. However, for exhaust ducts $-(1/2)F\theta_0$ is negative and first causes an increase in θ/θ_0 before the last term $(F\theta_0)^2$ takes over and causes a fall-off. This behavior can be seen in Fig. 7(a).

Concluding Remarks

With the optimum impedance information presented here and the spinning mode damping information of

Ref. 1, a design procedure for open circular inlet ducts was formulated which accounts for most of the important effects in the propagation of sound in a conventional acoustic liner.

Some limitations of the procedure should, however, be recognized. Only propagating modes were considered in the development. When a mode is very near or below cut-off, some of the simplified expressions (such as Eqs. (32), and (33)) begin to lose validity. A rotation of the equal damping contours (see Ref. 1) occurs as well as the expansion ($M_0 < 0$) or contraction ($M_0 > 0$) considered here. Also very near mode cut-off, the no end-reflection assumption may cause problems. A uniform boundary layer was assumed here. In practice, of course, the boundary layer is growing with length. Average values or stepped liners could be used to approximately account for this growth.

A $1/7^{th}$ power velocity profile away from the wall, merging into linear profile near the wall was assumed in the calculations. This was felt to be a reasonable approximation to what may be encountered in a real inlet. All of the correlations are presented using the $1/7^{th}$ power boundary layer thickness (δ). If a boundary layer displacement thickness is available approximate δ by $\delta = 8\delta^*$.

Further study will be required to determine the sound refraction effects on the optimum impedance of exhaust ducts. Although very little sensitivity to refraction was evident with the velocity profile used in this study, it is possible that a more realistic profile (for exhaust ducts) may produce a more significant effect.

The calculations in this paper are for the optimum impedance values which are of use even in drawing inferences about attenuation results for off-optimum impedances. This can best be illustrated by an example. Suppose a calculation were being made using the parameters given on Fig. 2 with a value of $\theta/\eta = 1.05$ (which represents a resistance above the optimum) and $\chi/\eta = 0$. An attenuation coefficient $\sigma \approx 0.015$ would be calculated if a very small boundary layer thickness were used. As boundary layer thickness is increased the optimum point moves down (to lower resistance, see Fig. 3) and the equal attenuation contours (σ constant) move down with the optimum. This causes lower damping contours to be swept past the selected impedance (1.05, 0) used in the calculation. Thus the calculated attenuation would monotonically decrease with increasing boundary layer thickness. Now suppose that a lower resistance had been selected for the attenuation calculation, for instance $\theta/\eta = 0.55$ (less than the optimum) and $\chi/\eta = 0$. For very small boundary layers the calculation would yield $\sigma \approx 0.01$. Now as boundary layer thickness is increased the higher attenuation contours near the optimum would be swept by the impedance of interest (0.55, 0) and the attenuation calculation would at first increase. When the optimum impedance has passed below (due to increased boundary layer thickness) the selected impedance the attenuation calculation would then show a fall-off in σ. Thus the attenuation has first increased and then decreased as boundary layer thickness was increased. From these two examples it is seen that the trend of attenuation with boundary layer thickness for off-optimum impedances depends upon the relationship of the impedance to the optimum impedance.

Conclusions

A wide ranging parametric study was presented which considered the effect of boundary layer refraction on the optimum acoustic impedance of the least attenuated spinning mode and a limited number of higher radial modes in a circular duct. The following conclusions were made.

1. Extremely large reductions in optimum acoustic resistance can occur due to the effect of an inlet steady flow boundary layer. The refraction effect of the boundary layer is less pronounced for the optimum acoustic reactance.

2. Boundary layer refraction effects are increased in inlets for increasing Mach numbers, frequencies, and boundary layer thickness. Inlet refraction effects are diminished for higher order circumferential and radial modes.

3. A correlation equation was derived, mainly from theoretical considerations, which adequately compares with the more exact calculations for an inlet.

4. The correlation equation was found to be adequate for higher order radial modes.

5. From the correlation, a boundary layer refraction parameter was developed which indicates whether or not refraction should be considered in the design of a specific inlet suppressor.

6. There is not much inherent loss of peak attenuation in an optimized design inlet due to boundary layer refraction. That is the maximum possible attenuation of a particular mode is a very weak function of boundary layer thickness until extremely high thicknesses are encountered. The optimum inlet design may have to be altered to account for refraction effects in order to maintain the peak sound attenuation at a high level.

7. The effect of boundary layer refraction on the optimum wall impedance in an exhaust duct is much less than for an inlet if all conditions (except flow direction) are the same.

Appendix - Development of Correlation Equations

The purpose of this development is to derive a correlation which can be used to unify the optimum impedance calculation results which were obtained by numerical integration in the body of this paper.

The starting point is an equation from Ref. 8 which expresses an approximate solution for the propagation of sound in a boundary layer velocity gradient and is valid for thin boundary layer thickness. This equation valid at the boundary layer edge is

$$\left.\frac{1}{p}\frac{dp}{d\xi}\right]_{\xi=1-\epsilon} = \frac{-(1 - M_0K)^2\left[ikr_0\overline{A} + \epsilon\left(\overline{\beta}I_1 - \overline{\alpha}\right)\right]}{1 + i\epsilon kr_0\overline{A}I_2} \qquad (A-1)$$

where

$$\epsilon = \frac{\delta}{r_0} \qquad (A-2)$$

$$\overline{\beta} = (kr_0)^2 K^2 + m^2 \qquad (A-3)$$

$$\overline{\alpha} = -ikr_0\overline{A} + (kr_0)^2 \qquad (A-4)$$

$$\overline{A} = \frac{1}{\zeta} \qquad (A-5)$$

The quantity $\overline{A}$ is the acoustic admittance at the wall, and I_1 and I_2 are integrals over the boundary layer given by

$$I_1 = \int_0^1 \frac{d\overline{y}}{(1 - M_0KG)^2} \qquad (A-6)$$

$$I_2 = \int_0^1 (1 - M_0KG)^2\, d\overline{y} \qquad (A-7)$$

The coordinate $\overline{y}$ is the nondimensional distance from the wall (y/δ). The function G represents the boundary layer shape and for a $1/7^{th}$ power low velocity profile is given by

$$G(\overline{y}) = \overline{y}^{1/7} (0 \le \overline{y} \le 1) \qquad (A-8)$$

Several simplifying assumptions and two fortuitous observations enabled the development of this complicated expression into a reasonably simple correlation expression. First, it was noted that the damping (σ) and propagation (τ) coefficients did not significantly change at the least attenuation mode optimum impedance point as the boundary layer thickness was increased. This implies that the eigenvalue (note: α not $\overline{\alpha}$) is also not a strong function of boundary layer thickness (see Eq. (12)) which in turn implies that the left hand side of Eq. (A-1) can be considered constant for changes in ϵ. This last implication evolves from Eqs. (13) and (14).

With $1/p\ dp/d\xi$ a constant at the boundary layer edge, the right side of Eq. (A-1) is used twice at zero thickness and at ϵ to form the equality

$$i\pi\eta\overline{A}_0 = \frac{i\pi\eta\overline{A} + \epsilon\left[\beta I_1 + i\pi\eta\overline{A} - (\pi\eta)^2\right]}{1 + i\epsilon\pi\eta\overline{A}I_2} \qquad (A-9)$$

where $\overline{A}_0$ is the optimum wall admittance at $\epsilon = 0$, while $\overline{A}$ is that at a finite ϵ. The quantity $(1 - M_0K)^2$ was cancelled since K does not vary if σ and τ are nearly constant. Use was made of the expression

$$kr_0 = \pi\eta \qquad (A-10)$$

Equation (A-9) can be rearranged and using $\overline{A} = 1/\zeta$ there results

$$\zeta = \frac{(1 + \epsilon)\zeta_0 - i\epsilon\pi\eta I_2}{1 - i\epsilon\pi\eta\left[1 - \dfrac{\overline{\beta}I_1}{(\pi\eta)^2}\right]\zeta_0} \qquad (A-11)$$

Equation (A-11) expresses the optimum wall impedance with a finite (but small) boundary layer thickness ($\epsilon = \delta/r_0$) in terms of the familiar (see Ref. 1) uniform or slip flow optimum wall impedance. This is useful provided the other terms in the expression can be evaluated.

The next step is to evaluate the integrals I_1 and I_2 which will require some simplifications. We will limit the development to propagating modes so that (see Ref. 1) a first order approximation for K is

$$K = \tau - i\sigma \approx \frac{1}{1 + M_0} \qquad (A-12)$$

Thus I_1 and I_2 can be written (using also (A-8))

$$I_1 = (1 + M_0)^2 \int_0^1 \frac{d\overline{y}}{\left[1 + M_0(1 - \overline{y}^{1/7})\right]^2} \qquad (A-13)$$

and

$$I_2 = \frac{1}{(1 + M_0)^2} \int_0^1 \left[1 + M_0(1 - \overline{y}^{1/7})\right]^2 d\overline{y} \qquad (A-14)$$

To this author's knowledge, I_1 cannot be evaluated in closed form but of course I_2 can be. Upon integrating I_1 numerically, the second fortunate occurrence was observed. It was found that up to $|M_0| = 0.8$

$$I_1 \approx \frac{1}{I_2} \qquad (A-15)$$

with an error of less than 9 percent. Equation (A-15) was found to be approximately true also for a linear boundary layer with slip where both integrals can be evaluated in closed form.

The closed form expression for I_2 with a $1/7^{th}$ velocity profile is

$$I_2 = \frac{\left[1 + \frac{M_0}{4}\left(1 + \frac{M_0}{9}\right)\right]}{(1 + M_0)^2} \qquad \text{(A-16)}$$

which is Eq. (28) in the main text. The integral I_1 is then taken as the reciprocal of Eq. (A-16).

Let F denote the quantity in the denominator of Eq. (A-11) and use Eqs. (A-3) and (A-4) to yield

$$F = \frac{\epsilon\pi\eta}{I_2}\left\{I_2 - \left[K^2 + \left(\frac{m}{\pi\eta}\right)^2\right]\right\} \qquad \text{(A-17)}$$

To evaluate F a second order approximation to K^2 must be used (since $m/\pi\eta$ also small). From Ref. 1 one can derive (for propagating modes)

$$K \approx \frac{1}{1 + m_0} - \frac{1}{2}\left(\frac{R}{\pi\eta}\right)^2 (\cos 2\varphi + i \sin 2\varphi) \qquad \text{(A-18)}$$

where R and φ are the mode eigenvalue magnitude and phase at the optimum impedance. Since φ is usually small at the optimum (Table II of Ref. 1)

$$\cos 2\varphi > \sin 2\varphi \qquad \text{(A-19)}$$

and the last term of Eq. (A-18) will be ignored. Thus

$$K^2 \approx \frac{1}{(1 + M_0)^2} - \frac{\left(\frac{R}{\pi\eta}\right)^2 \cos 2\varphi}{1 + M_0} \qquad \text{(A-20)}$$

and Eq. (A-17) can be written

$$F = \frac{2\pi(\delta/\lambda)}{I_2}\left[\frac{M_0\left(1 + \frac{M_0}{9}\right)}{4(1 + M_0)^2} + \frac{\left(\frac{R}{\pi\eta}\right)^2 \cos 2\varphi}{(1 + M_0)} - \left(\frac{m}{\pi\eta}\right)^2\right] \qquad \text{(A-21)}$$

where

$$\epsilon = \frac{2}{\pi}\left(\frac{\delta}{\lambda}\right) \qquad \text{(A-22)}$$

was used.

This is about as far as the approximate theory could be carried (Eq. (A-21)). From here on comparisons must be made with the more exact calculations made in the main text. When the real part of Eq. (A-11) (using F in the denominator) was compared to the calculated points in Fig. 4, it was immediately evident that the second term in the numerator of Eq. (A-11) had to be deleted. This term $(-i\epsilon\pi\eta I_2)$ causes θ/θ_0 to go negative at moderate boundary layer thickness. Deleting this term in effect is deleting the small term in the denominator $(i\epsilon kr_0\bar{A} I_2)$ of Eq. (A-1) which may have implications in the use of Eversman's result for moderate boundary layer thickness.

The modified form of Eq. (A-11) is then

$$\zeta = \frac{(1 + \epsilon)\zeta_0}{1 - iF\zeta_0} \qquad \text{(A-23)}$$

which is Eq. (26) in the main text. Now if Eq. (A-23) is used with F from Eq. (A-21) retaining only the first term in brackets, a quite acceptable fit of the results in Fig. 4 is obtained. However, the agreement between the exact calculation and the correlation can be improved by using small empirical corrections. This is not surprising due to all of the approximations made to this point. The simplest possible corrections were made (linear corrections) and somewhat more sophisticated curve-fitting procedures could probably improve the correlation even more.

A Mach number multiplier was inserted into the first term of Eq. (A-21). This correction term was $1/2(1 - 2M_0)$ which ranges from 0.7 to 1.3 as Mach number varies between -0.2 and -0.8.

The second empirical correction was made to the second term of Eq. (A-21) which involves the quantity $R^2 \cos 2\varphi$ which is the real part of the square of the eigenvalue. This is a function of the circumferential lobe number as well as the radial mode number. Rather than inserting the actual values of R and φ, the term was considered empirically as a function of the lobe number (m). The empirical substitute obtained was $(1/2)m^2$.

With these two empiricisms inserted, Eq. (A-21) becomes (also use $m_0/9 \ll 1$)

$$F = \frac{\pi(\delta/\lambda)}{4I_2(1 + M_0)^2}\left[M_0(1 - 2M_0) - 4(1 + 2M_0)(1 + M_0)\left(\frac{m}{\pi\eta}\right)^2\right] \qquad \text{(A-24)}$$

which is Eq. (27) in the main text.

The intent in this appendix was to develop a boundary layer refraction effect correlation which was as theoretically based as possible. In this way the major effects of the parameters would appear in their correct functional form with a minimum of guesswork which usually accompanies a correlation. Small empirical corrections were then applied to improve the correlation. The final form of the equation would probably never have been derived from purely empirical curve-fitting.

References

1. Rice, E. J., "Spinning Mode Sound Propagation in Ducts with Acoustic Treatment," presented at the 88th Acoustical Society of America Meeting, St. Louis, Mo., Nov. 1974; NASA TM X-71613; also NASA TN D-7913.

2. Pridmore-Brown, D. C., "Sound Propagation in a Fluid Flowing Through an Attenuating Duct," Journal of Fluid Mechanics, Vol. 4, Pt. 4, Aug. 1958, pp. 393-406.

3. Mungur, P. and Plumblee, H. E., "Propagation and Attenuation of Sound in a Soft-Walled Annular Duct Containing a Sheared Flow," Basic Aerodynamic Noise Research, SP-207, 1969, NASA, pp. 305-327.

4. Nayfeh, A. H., Kaiser, J. E. and Telionis, D. P., "The Acoustics of Aircraft Engine-Duct Systems," AIAA Paper 73-1153, Montreal, Canada, 1973.

5. Ko, S.-H., "Sound Attenuation in Acoustically Lined Circular Ducts in the Presence of Uniform Flow and Shear Flow," Journal of Sound and Vibration, Vol. 22, No. 2, May 1972, pp. 193-210.

6. Schauer, J. J. and Hoffman, E. P., "Optimum Duct Wall Impedance Shear Sensitivity," AIAA Paper 75-129, Pasadena, Calif., 1975.

7. Yurkovich, R. N., "Attenuation of Acoustic Modes in Circular and Annular Ducts in the Presence of Sheared Flow," AIAA Paper 75-131, Pasadena, Calif., 1975.

8. Eversman, W. and Beckemeyer, R. J., "Transmission of Sound in Ducts with Thin Shear Layers-Convergence to the Uniform Flow Case," The Journal of the Acoustical Society of America, Vol. 52, No. 1, July 1972, pp. 216-220.

9. Morfey, C. L., "A Note on the Radiation Efficiency of Acoustic Duct Modes," Journal of Sound Vibration, Vol. 9, No. 3, May 1969, pp. 367-372.

10. Goldstein, M. and Rice, E. J., "Effect of Shear on Duct Wall Impedance," Journal of Sound Vibration, Vol. 30, No. 1, Sept. 1973, pp. 79-84.

11. Nayfeh, A. H., Kaiser, J. E., and Shaker, B. S., "Effect of Mean-Velocity Profile Shapes on Sound Transmission Through Two-Dimensional Ducts," Journal of Sound and Vibration, Vol. 34, No. 3, June 1974, pp. 413-423.

12. Schlichting, H., Boundary Layer Theory, McGraw-Hill, New York, 1955.

TABLE I. - OPTIMUM RESISTANCE AND REACTANCE COEFFICIENTS FOR SPINNING MODES IN CIRCULAR DUCTS

m	0	1	3	5	7	10	20	50
B_0	0.890	0.644	0.448	0.357	0.303	0.251	0.170	0.097
B_X	0.38	0.221	0.121	0.095	0.076	0.060	0.038	0.020

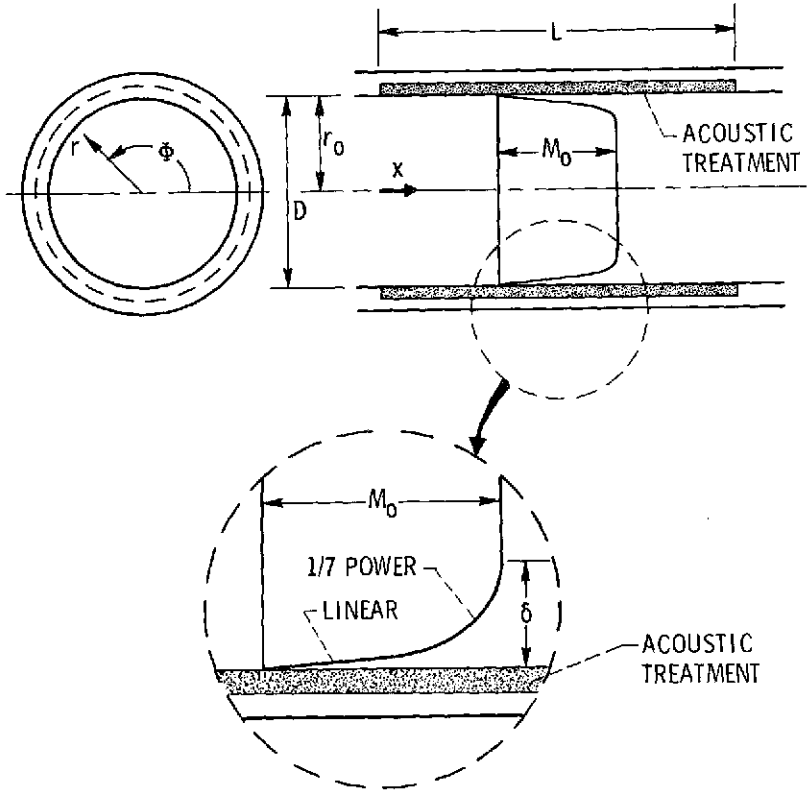

Figure 1. - Geometry and steady-flow velocity profile.

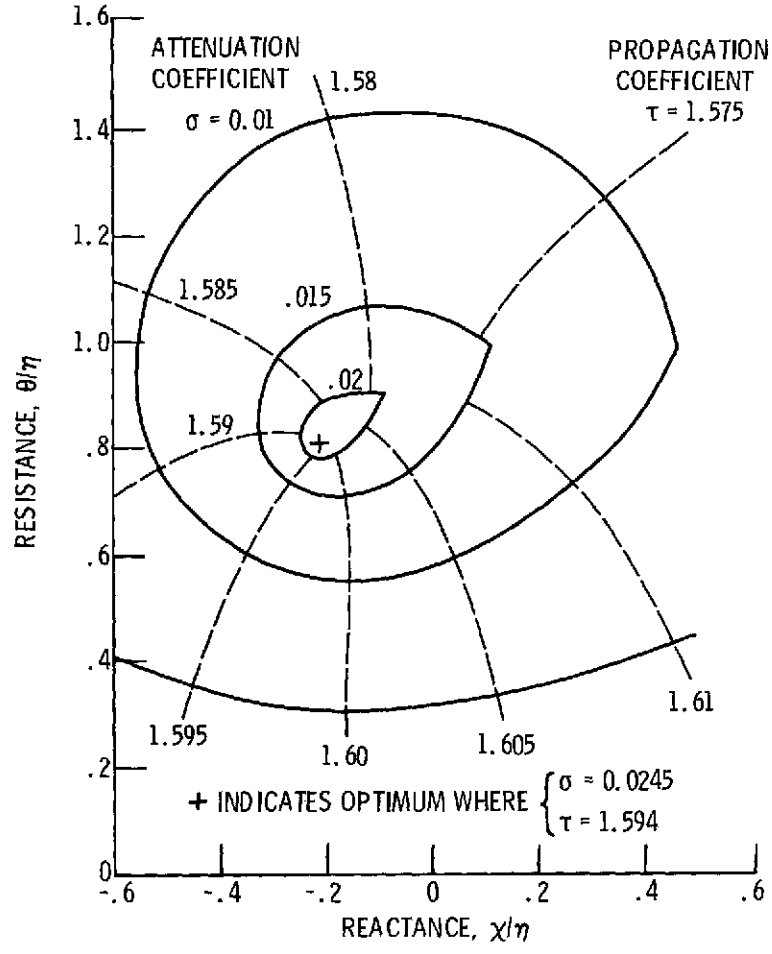

Figure 2. - Constant attenuation and propagation contours for the least attenuated spinning mode using displacement boundary condition. Inlet Mach number, $M_0 = -0.4$; lobe number, $m = 7$; frequency parameter, $\eta = 10$; boundary layer thickness, $\delta/r_0 = 0$.

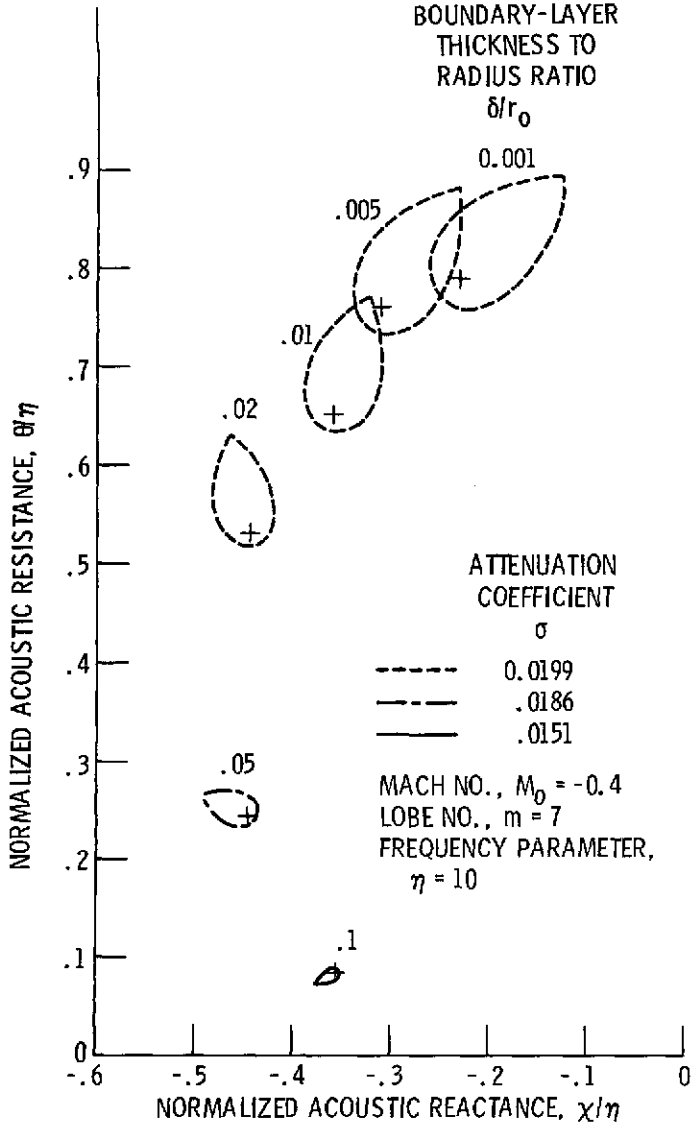

Figure 3. - Constant attenuation contours for several boundary layer thicknesses (δ/r_0) for the least attenuated spinning mode.

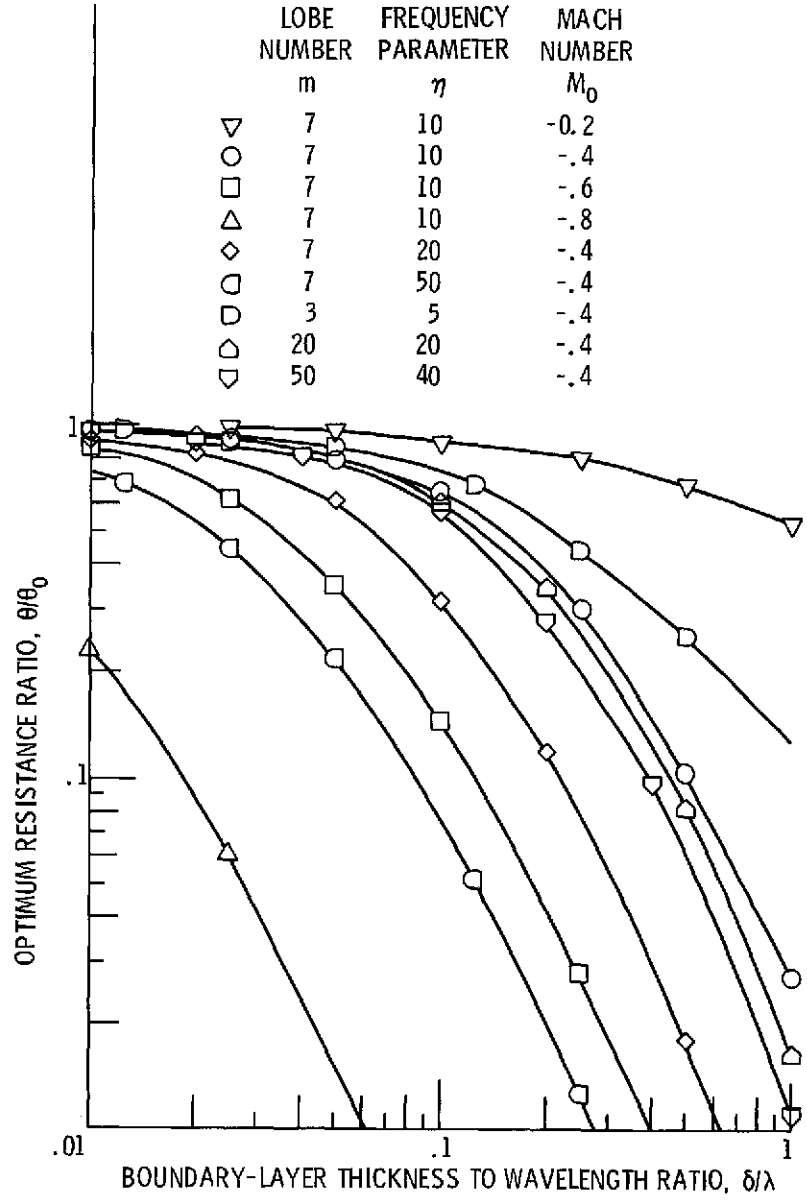

Figure 4. - Effect of boundary layer on inlet optimum resistance ratio for the least attenuated spinning mode with lobe number, frequency parameter, and Mach number as parameters.

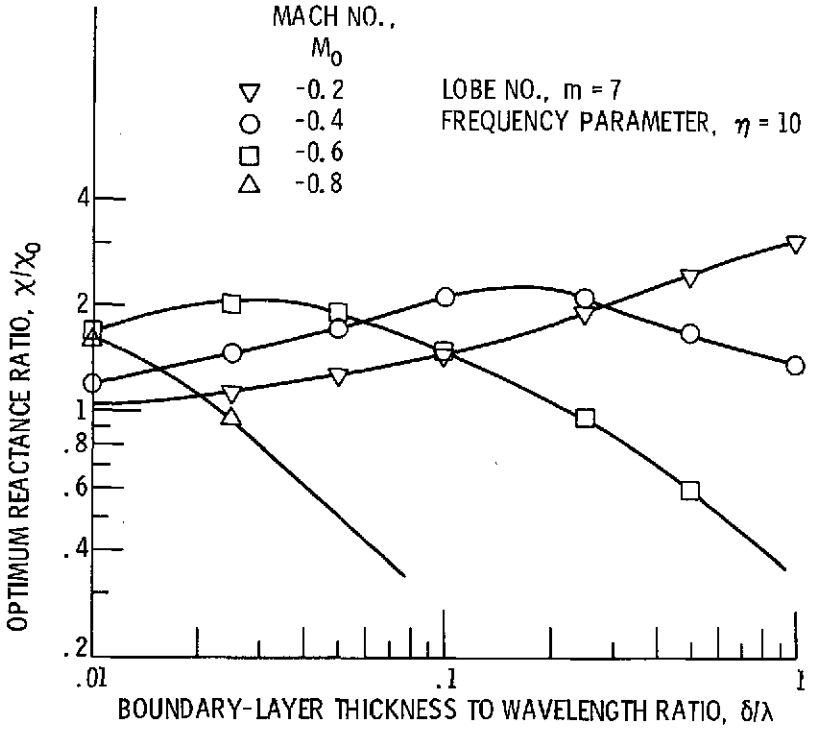

Figure 5. - Effect of boundary layer on inlet optimum reactance ratio for the least attenuated spinning mode with Mach number as a parameter.

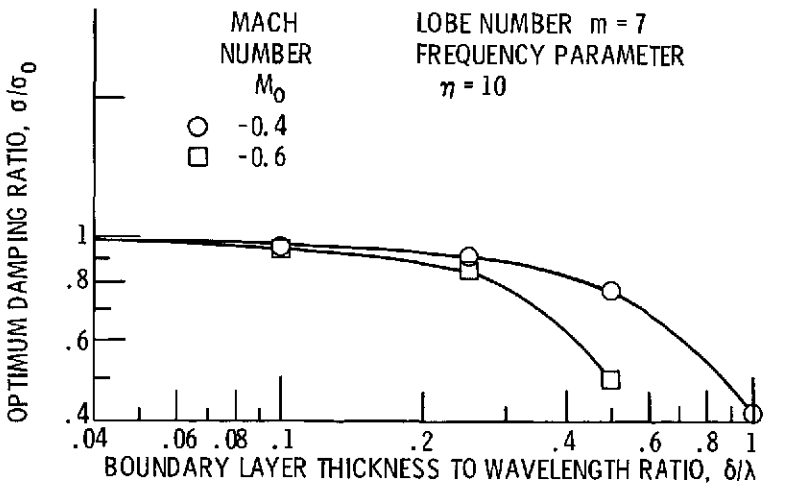

Figure 6. - Effect of boundary layer on inlet optimum damping ratio for the least attenuated spinning mode.

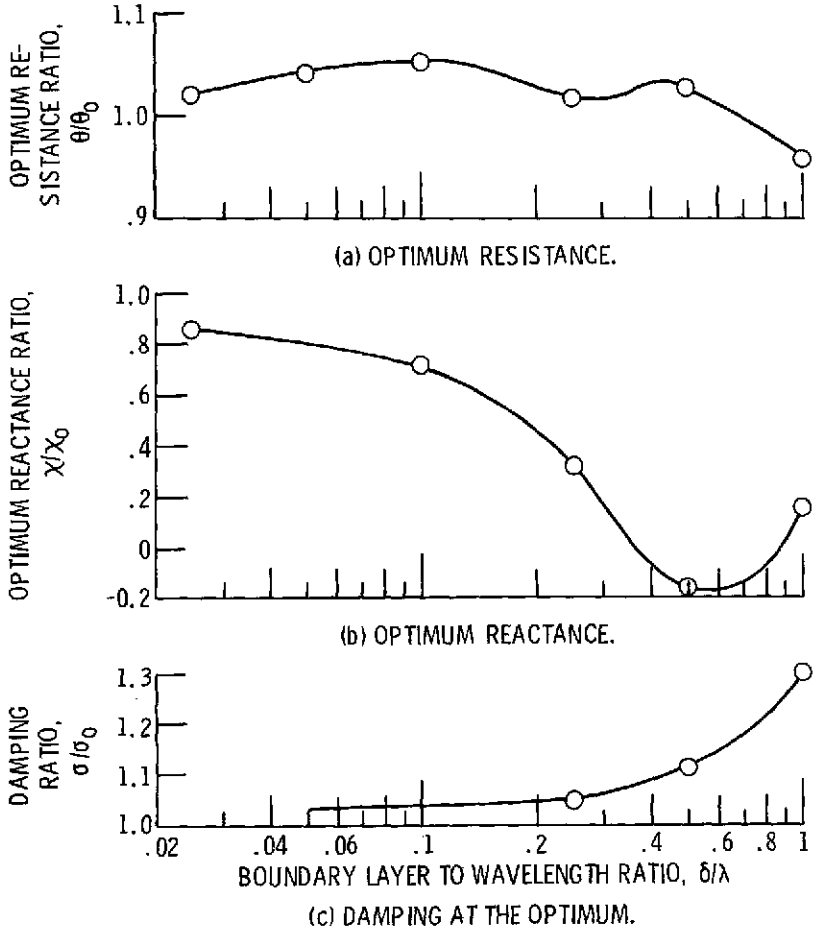

Figure 7. - Exhaust duct optimum resistance, reactance, and damping as a function of boundary-layer thickness. Least attenuated mode, lobe number m = 7, frequency parameter $\eta = 10$, Mach number $M_0 = 0.6$.

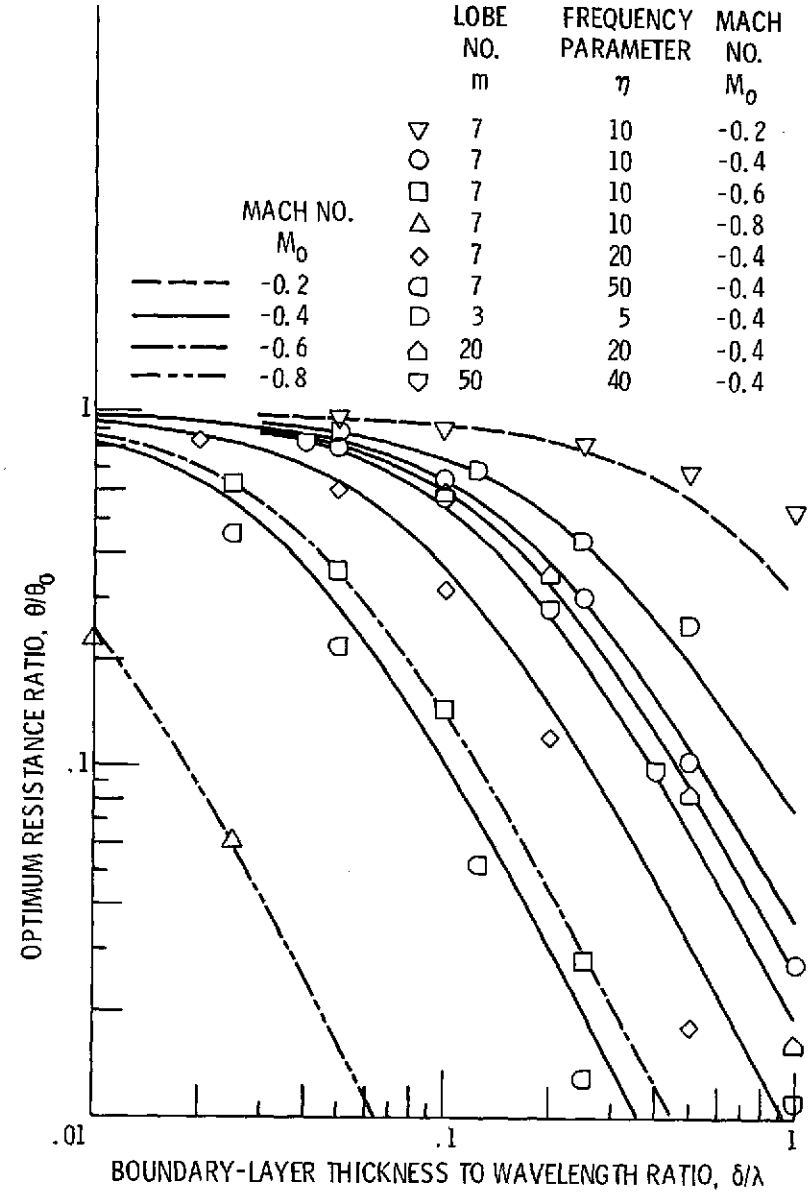

Figure 8. - Optimum resistance ratio, comparison between exact calculations and correlation for inlets for the least attenuated spinning mode.

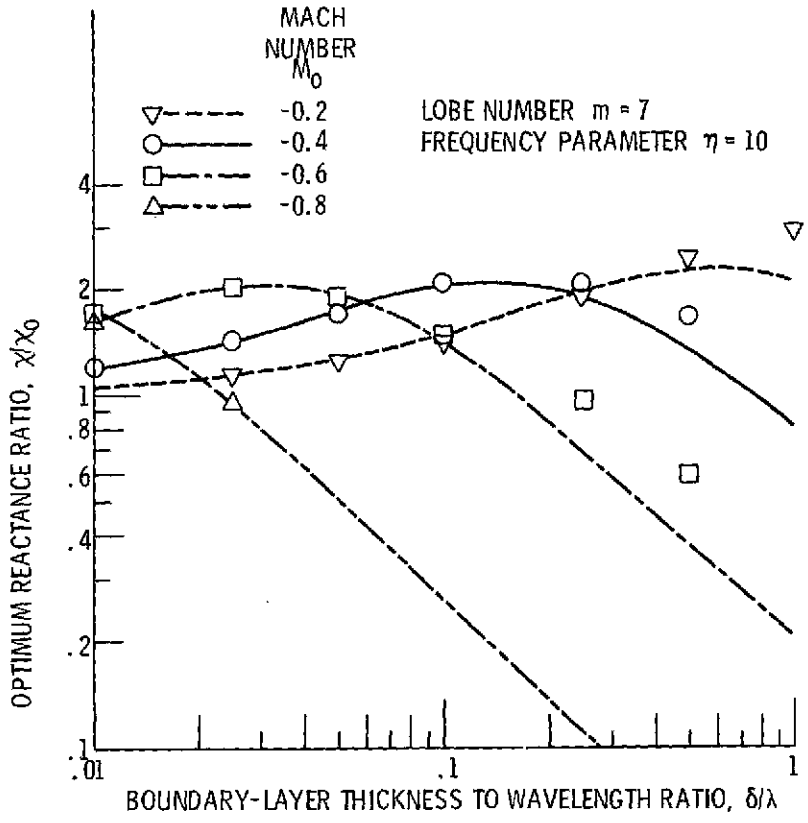

Figure 9. - Optimum reactance ratio, comparison between exact calculations and correlation for inlets for the least attenuated spinning mode.

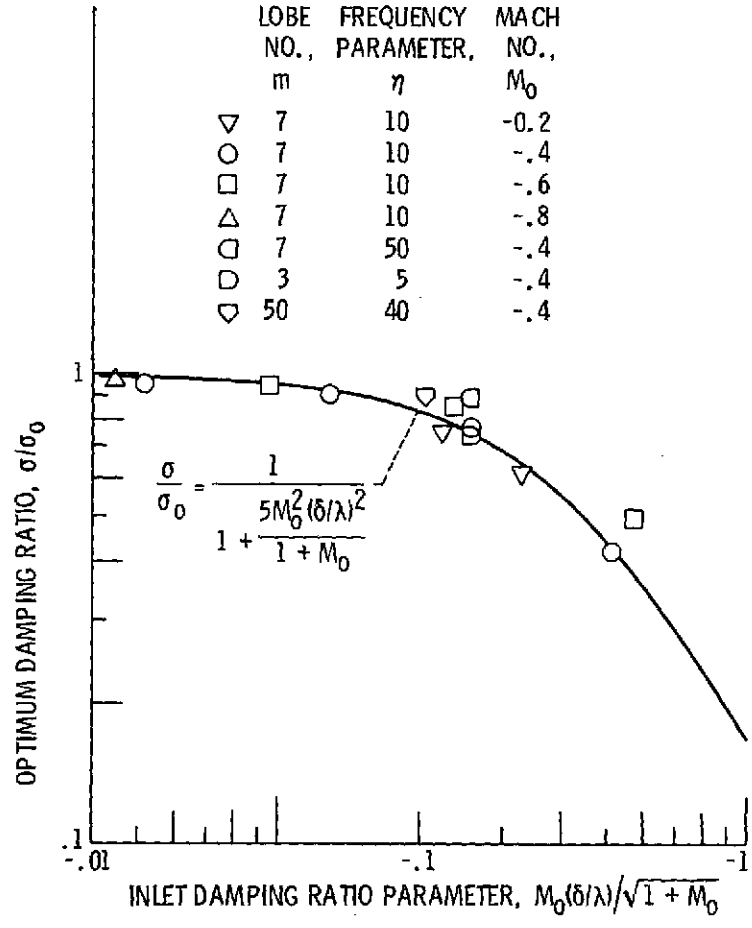

Figure 10. - Optimum damping ratio, comparison between exact calculation and correlation for inlets for the least attenuated spinning mode.

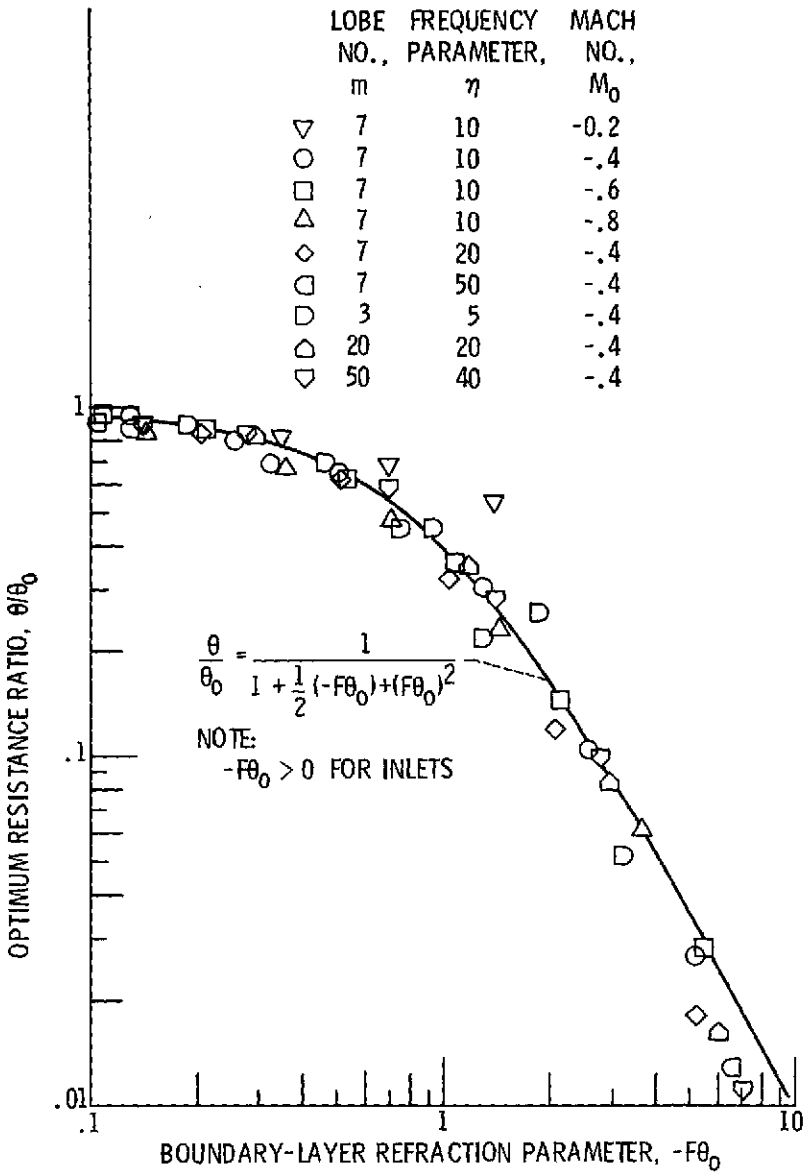

Figure 11. - Inlet optimum resistance ratio for the least attenuated spinning mode, unification of calculations using boundary-layer refraction parameter.

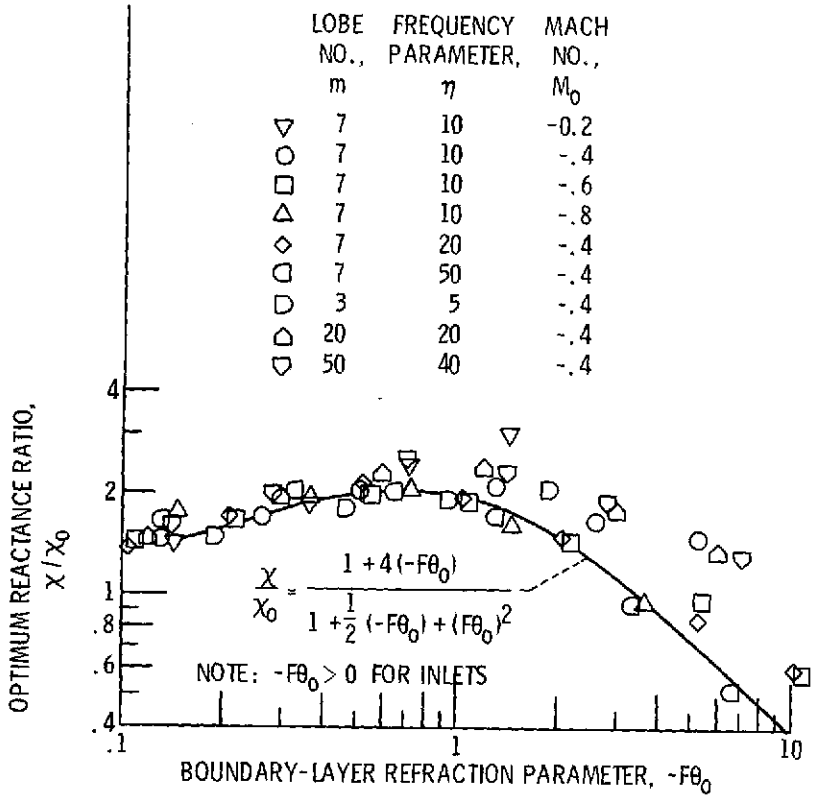

Figure 12. - Inlet optimum reactance ratio for the least attenuated spinning mode, unification of calculations using boundary-layer refraction parameter.

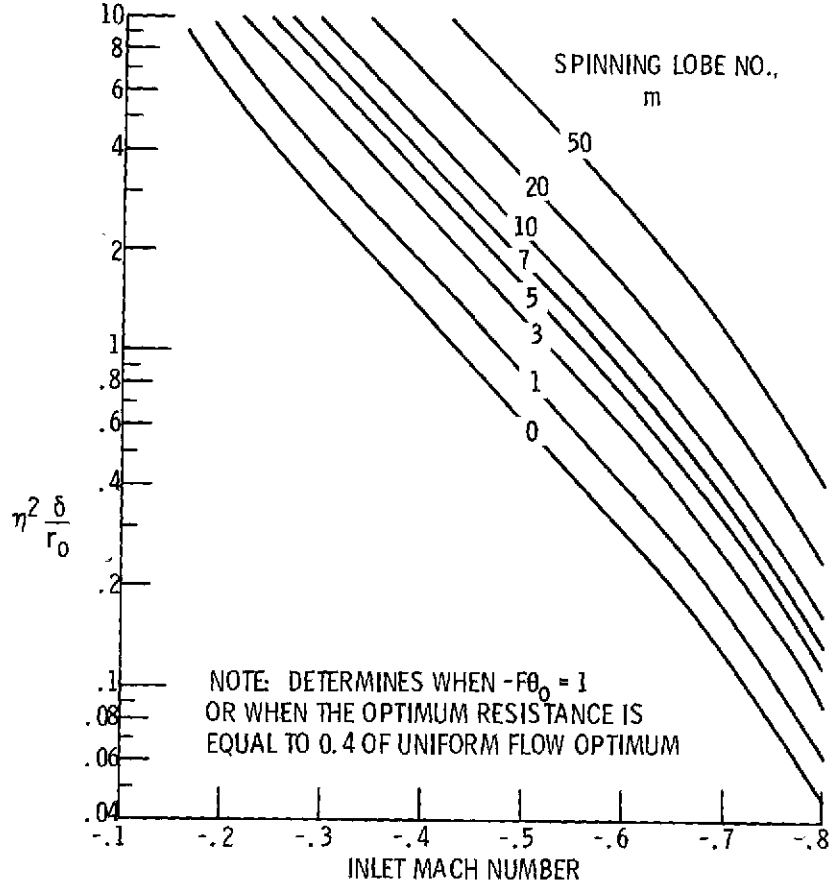

Figure 13. - Nomograph for onset of significant boundary-layer sound refraction effect on optimum resistance.

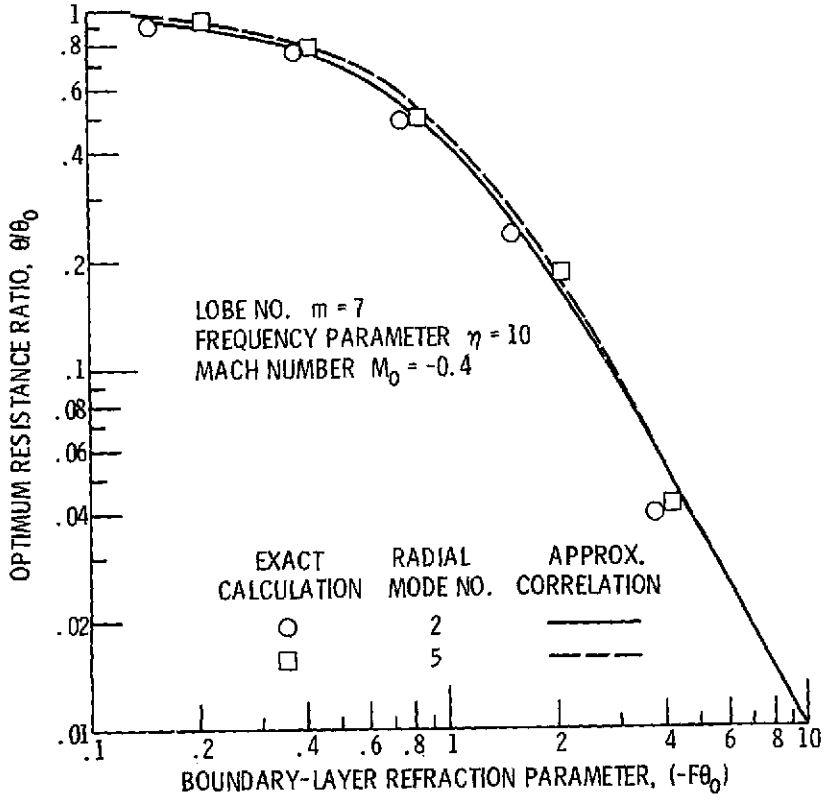

Figure 14. - The effect of inlet boundary layer on the optimum resistance ratio for higher order radial modes.

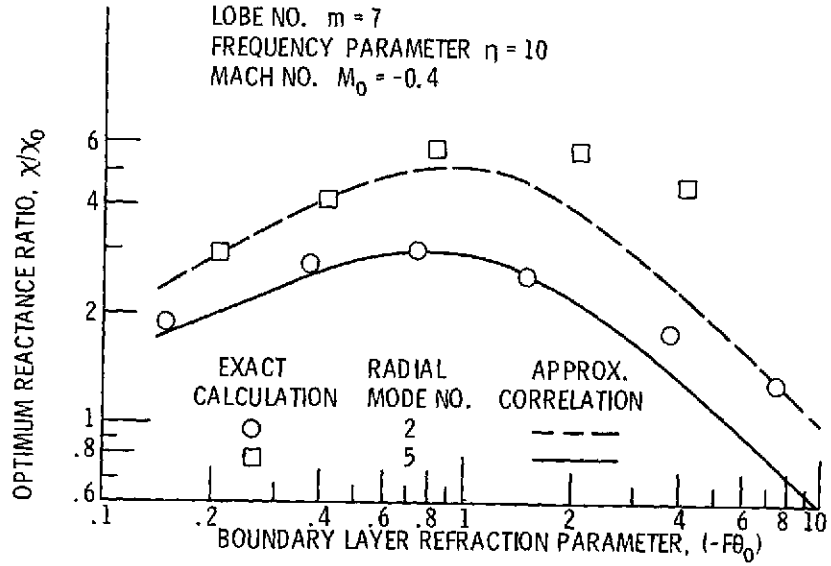

Figure 15. - The effect of inlet boundary layer on the optimum reactance ratio for higher order radial modes.